



OPEN

## In vivo electrical conductivity measurement of muscle, cartilage, and peripheral nerve around knee joint using MR-electrical properties tomography

Ji Hyun Lee<sup>1</sup>, Young Cheol Yoon<sup>1</sup>✉, Hyun Su Kim<sup>1</sup>, Jiyeong Lee<sup>1</sup>, Eunju Kim<sup>2</sup>, Christian Findekle<sup>3</sup> & Ulrich Katscher<sup>3</sup>

This study aimed to investigate whether in vivo MR-electrical properties tomography (MR-EPT) is feasible in musculoskeletal tissues by evaluating the conductivity of muscle, cartilage, and peripheral nerve around the knee joint, and to explore whether these measurements change after exercise. This prospective study was approved by the institutional review board. On February 2020, ten healthy volunteers provided written informed consent and underwent MRI of the right knee using a three-dimensional balanced steady-state free precession (bSSFP) sequence. To test the effect of loading, the subjects performed 60 squatting exercises after baseline MRI, immediately followed by post-exercise MRI with the same sequences. After reconstruction of conductivity map based on the bSSFP sequence, conductivity of muscles, cartilages, and nerves were measured. Measurements between the baseline and post-exercise MRI were compared using the paired *t*-test. Test–retest reliability for baseline conductivity was evaluated using the intraclass correlation coefficient. The baseline and post-exercise conductivity values (mean  $\pm$  standard deviation) [S/m] of muscles, cartilages, and nerves were  $1.73 \pm 0.40$  and  $1.82 \pm 0.50$  ( $p = 0.048$ ),  $2.29 \pm 0.47$  and  $2.51 \pm 0.37$  ( $p = 0.006$ ), and  $2.35 \pm 0.57$  and  $2.36 \pm 0.57$  ( $p = 0.927$ ), respectively. Intraclass correlation coefficient for the baseline conductivity of muscles, cartilages, and nerves were 0.89, 0.67, and 0.89, respectively. In conclusion, in vivo conductivity measurement of musculoskeletal tissues is feasible using MR-EPT. Conductivity of muscles and cartilages significantly changed with an overall increase after exercise.

### Abbreviations

|       |                                       |
|-------|---------------------------------------|
| EIT   | Electrical impedance tomography       |
| EPT   | Electrical properties tomography      |
| RF    | Radiofrequency                        |
| SAR   | Specific absorption rate              |
| RT    | Relaxation time                       |
| DTI   | Diffusion tensor imaging              |
| 3D    | Three-dimensional                     |
| bSSFP | Balanced steady-state free precession |
| bFFE  | Balanced fast field echo              |
| ROI   | Region of interest                    |
| VM    | Vastus medialis                       |
| SM    | Semimembranosus                       |
| BF    | Biceps femoris                        |
| FA    | Fractional anisotropy                 |

<sup>1</sup>Department of Radiology, Samsung Medical Center, Sungkyunkwan University School of Medicine, 81 Irwon-ro, Gangnam-gu 06351, Seoul, Korea. <sup>2</sup>Philips Korea, Seoul, Korea. <sup>3</sup>Philips Research Hamburg, Hamburg, Germany. ✉email: youngcheol.yoon@gmail.com

MD Mean diffusivity  
ICC Intraclass correlation coefficient

Electrical conductivity is an intrinsic property of a material that represents the capability to transfer electrical current inside the medium<sup>1</sup>. In biological tissues, it is closely related to water content, intracellular and extracellular fluid volumes, ion concentration, and the cellular membrane permeability, thus has been considered to be a fundamental biophysical property<sup>2,3</sup>. As several experimental studies have shown that conductivity can reflect pathologic status as well as tissue type<sup>4–7</sup>, it has emerged as a potentially important tissue biomarker for clinical diagnostics<sup>8,9</sup>.

While previous investigations mostly relied on ex vivo measurements<sup>4–7</sup>, the first non-invasive in vivo assessment of conductivity was made using the electrical impedance tomography (EIT)<sup>10</sup>. Among multiple efforts to improve non-invasive conductivity imaging, MR-EIT provided higher spatial resolution and eliminated the need to solve the ill-posed inverse problem in EIT<sup>11</sup>. However, as it required injection of electrical current into the body, safety concerns were raised<sup>9</sup>. Another technique called magnetic induction tomography did not involve direct contact with the subject, nevertheless, this non-MRI-based method exhibited poor spatial resolution<sup>12</sup>.

Based on the concept of deriving conductivity from the measured MR signals<sup>13</sup>, another non-invasive approach termed “MR-electrical properties tomography (MR-EPT)” has been introduced by Katscher et al.<sup>14</sup>. They reconstructed tissue conductivity from the measured  $B_1^+$  field generated by the radiofrequency (RF) coil. It is considered to be advantageous regarding practicability, as it can be acquired using standard MRI system with a regular coil and does not apply externally mounted electrodes or current<sup>8</sup>. With increasing interest, there has been continuous progress in the research of MR-EPT to validate it<sup>15</sup>, prove its feasibility<sup>16</sup>, and estimate specific absorption rate (SAR)<sup>17</sup>. Whilst several clinical studies have investigated MR-EPT in various organs including breast<sup>18,19</sup>, brain<sup>20</sup>, and liver<sup>21</sup>, the number of studies that utilized MR-EPT in musculoskeletal tissues has been limited<sup>22</sup>.

Thus, the purpose of this study was to investigate whether in vivo imaging is feasible in musculoskeletal tissues using MR-EPT by evaluating the conductivity of muscle, cartilage, and peripheral nerves around the knee joint. Under the hypothesis that conductivity could reflect physiologic changes, this study also sought to explore whether the conductivity of musculoskeletal tissues changes after exercise, and to interpret their changes with reference to other quantitative measurements including T2, T2\* relaxation times (RT) and diffusion tensor imaging (DTI) parameters.

## Materials and methods

This prospective study was approved by the institutional review board (Samsung Medical Center, IRB File No. 2019-11-032) and registered at [cris.nih.go.kr](https://cris.nih.go.kr) (KCT0004839). After being advised of the purpose of the study, all subjects gave written informed consent. The study was conducted in accordance with the declaration of Helsinki.

**Study population.** According to a previous study<sup>22</sup>, the mean and standard deviation of muscle conductivity using MR-EPT has been reported to be 0.93 S/m (Siemens per meter =  $\Omega^{-1} \text{ m}^{-1}$ ) and 0.26 S/m, respectively. The sample size ( $n$ ) needed to construct a 95% confidence interval with a margin of error of 0.17 S/m was prospectively calculated using the following equation:  $n = 1.96^2 \times SD^2/d^2$ , where SD and  $d$  are the standard deviation of muscle conductivity and the margin of error, respectively. Therefore, the sample size was calculated to be nine. Assuming dropout rate to be 10%, ten subjects were required.

Ten healthy adults were recruited who had body mass index between 18.5 and 25.0, without any discomfort in their lower extremities, previous history of internal derangement, surgery in the right knee, or contraindication to MRI such as claustrophobia.

**Magnetic resonance imaging acquisition.** All volunteers underwent baseline imaging using a 3.0-T MRI scanner (Ingenia CX, Philips Medical Systems) and a 16-channel knee coil. For conductivity assessment, a three-dimensional (3D) balanced steady-state free precession (bSSFP) (balanced fast field echo [bFFE], Philips Medical Systems) sequence was chosen; this sequence was selected due to its relatively benign off-resonance behavior and robustness against unwanted phase contribution from flow, motion, and eddy current<sup>8</sup>. Both magnitude and phase images were obtained in the axial plane. To evaluate the test–retest reliability of conductivity, all volunteers underwent two iterations of the bSSFP sequence. Thereafter, T2 map (T2-weighted multi-echo spin-echo sequence), T2\* map (T2\*-weighted multi-echo fast-field echo sequence with  $\Delta B_0$  correction), and DTI (single-shot echo-planar imaging) in the axial planes were acquired. T2 and T2\* maps were computed using a pixel-by-pixel basis, mono-exponential, non-negative least-square fitting algorithm. For DTI, diffusion gradients were applied in six directions and diffusion encoding was done with monopolar gradient pulses. Detailed MRI parameters are summarized in Table 1.

**Exercise protocol and post-exercise imaging.** To test the effect of loading, the volunteers performed squatting exercise outside the MRI scanner after baseline imaging as described in a previous literature<sup>23</sup>. Standing with weight equally distributed and the feet separated shoulder width apart, they were asked to stand in a position of knee flexion at 90° bilaterally. Keeping the knees not moving past the toes, they held this position for 3 s, followed by repositioning to stand upright. They performed 60 repetitions under supervision by an observer to ensure identical exercise among the volunteers. After exercising, the volunteers were immediately repositioned on the MR table for post-exercise imaging using the same sequences and protocols as the baseline imaging, including two iterations of the bSSFP sequence. The first and second post-exercise bSSFP sequences were acquired 2 and 6 min after exercise cessation in all volunteers, respectively. Volunteers’ skin was marked

|                           | bSSFP      | T2 map      | T2* map           | DTI        |
|---------------------------|------------|-------------|-------------------|------------|
| TR (ms)                   | 4.5302     | 1735.2      | 61.8963           | 3399.1     |
| TE (ms)                   | 2.265      | 13 (13, 6)* | 2.83 (2.354, 15)* | 61.344     |
| Acquisition matrix        | 224 × 222  | 400 × 286   | 400 × 400         | 116 × 114  |
| Reconstruction matrix     | 352 × 352  | 400 × 400   | 448 × 448         | 128 × 128  |
| Pixel spacing (mm)        | 0.568      | 0.500       | 0.446             | 1.562      |
| Field of view (cm)        | 20         | 20          | 20                | 20         |
| Slice Thickness/gap (mm)  | 1/0        | 3/0.3       | 3/0.3             | 3/0        |
| b values                  | –          | –           | –                 | 0, 600     |
| Number of averages        | 2          | 1           | 1                 | 2          |
| Number of slices          | 80         | 20          | 20                | 30         |
| Echo train length         | 1          | 6           | 15                | 57         |
| Parallel reduction factor | 1          | 2           | 2.1               | 2          |
| Flip angle (°)            | 30         | 90          | 25                | 90         |
| Acquisition time          | 4 min 12 s | 4 min 9 s   | 3 min 14 s        | 3 min 34 s |

**Table 1.** Parameters of MR sequences. TR, repetition time; TE, echo time; bSSFP, balanced steady-state free precession; DTI, diffusion tensor imaging. \*Data are the first TE with  $\Delta$ TE and the number of TE values in parentheses.

under the guidance of integrated laser to maintain identical imaging position between the baseline and post-exercise imaging.

**EPT reconstruction.** After data acquisition, all images were transferred to an independent workstation for analysis with manufacturer-supplied software (Extended Philips Research Software Solution [EXPRESS], Philips Healthcare). The conductivity maps were reconstructed from the phase images of the 3D bSSFP sequence. To convert the phase information to conductivity ( $\sigma$ ), the following equation (assuming constant  $B_1$  magnitude) was used:

$$\sigma = \Delta\Phi^+ / (\mu\omega)$$

where  $\omega$  = Larmor frequency,  $\Delta$  = Laplacian operator,  $\mu$  = magnetic permeability of tissue (assumed to be equal to magnetic permeability of free space), and  $\Phi^+$  = RF transmit phase estimated as half of the measured transceive phase  $\Phi^\pm$  (i.e.,  $\Phi^+ \approx \Phi^\pm/2$ )<sup>8</sup>. Care has to be taken that  $\Phi^+$  does not show any phase wraps when applying this division by two. However, since the total phase span across the field of view has been roughly 60° for the experiments in this study, no dedicated phase unwrapping was needed. The second derivative required for  $\Delta$  was performed numerically by fitting a local parabola to a number  $N$  of voxels (“kernel”) on each side of the respective target voxel of  $\Phi^\pm$ . A maximum number of  $N$  was chosen as  $N_{\max} = 10$  and reduced as soon as the bSSFP magnitude of a kernel voxel deviates more than 10% from the target voxel, providing a suitable trade-off between too low signal-to-noise ratio (for too small  $N$ ) and decreased image resolution (for too large  $N$ ) and avoids the typical boundary artifacts of EPT. As the Laplacian operator inevitably leads to noise amplification, a bilateral median filter was applied to the conductivity resulting from those equations, again applying the locally shaped kernel as done for the differentiation step. This approach has successfully been applied in previous studies for brain tumor conductivity<sup>20,24</sup> and similarly also for breast tumor conductivity<sup>19,25</sup>.

**Image analysis.** Two board-certified radiologists (readers I and II; 5 and 1 years of experience in musculoskeletal imaging, respectively) analyzed the MRIs. Among T2-weighted images with six different echo times, one was selected and regarded as anatomical reference that best differentiated subchondral bone, articular cartilage, and joint fluid from the cartilage. Using the manufacturer-supplied software (Extended Philips Research Software Solution [EXPRESS], Philips), conductivities of muscles, cartilages, and nerves were measured by placing regions of interests (ROIs) on the magnitude image of the 3D bSSFP sequence using freehand drawing tools according to the following criteria (Fig. 1):

- (1) Muscles: At the level of the distal thigh, the vastus medialis (VM), semimembranosus muscles (SM), and biceps femoris muscle, including both long and short heads (BF) were selected because they had sufficient cross-sectional area. The ROIs were placed on each muscle so that the boundaries were within 1–2 mm from the muscle fascia.
- (2) Cartilages: Axial planes that revealed the maximum thickness of the patellar and trochlear cartilages were selected for evaluation. The ROIs were placed to cover the entire cartilage, encompassing both deep and superficial cartilage, and medial and lateral facets; joint fluid or subchondral bone were carefully avoided.
- (3) Nerve: At the same axial plane as that for muscle analysis, the ROIs were carefully drawn to fall within the visualized boundary of the tibial nerve, excluding the perineural vessels.

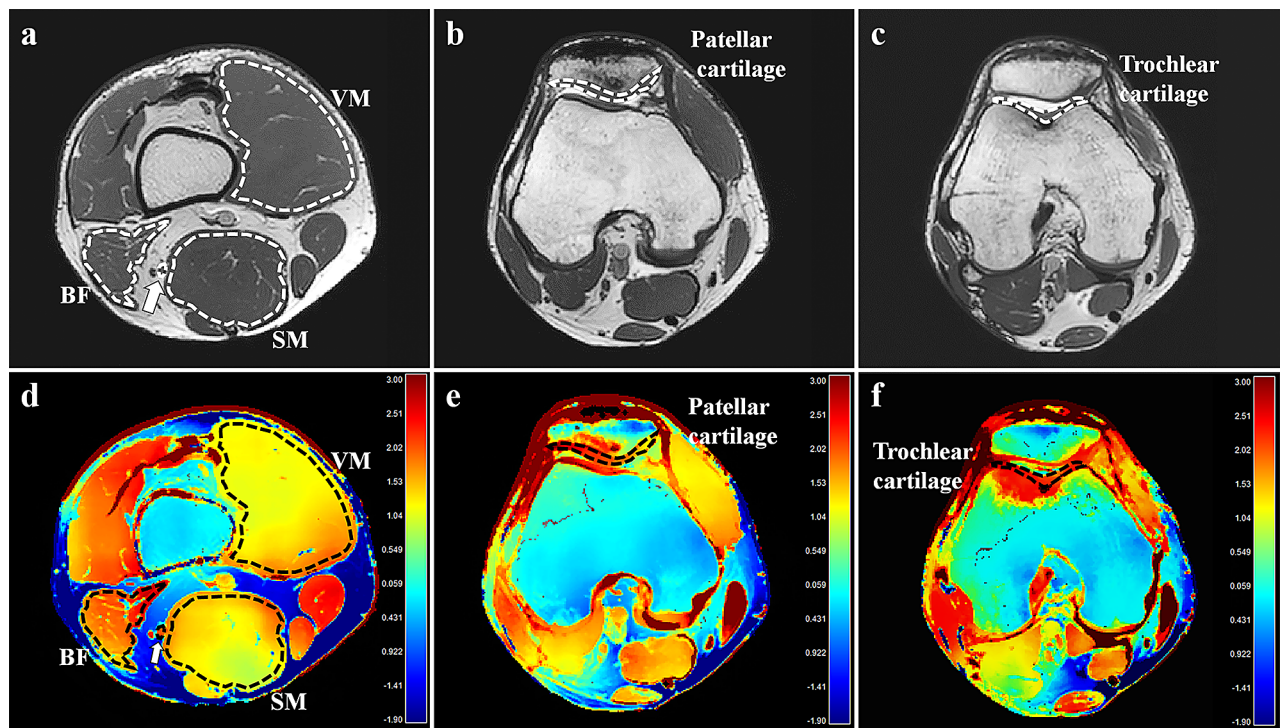


**Figure 1.** An example of conductivity analysis in the right knee of a 30-year old male volunteer. Regions of interest (ROIs) were placed in the vastus medialis (VM), semimembranosus (SM) muscles, biceps femoris muscle, including both long and short heads (BF), tibial nerve at the distal thigh level, and patellar and trochlear cartilage on the axial three-dimensional balanced fast-field echo sequence (a–c). ROIs with identical shapes, sizes, and positions were automatically generated on the conductivity map (d–f). The unit for the scale bars is S/m. Arrows, tibial nerve; dotted lines, ROIs.

Dedicated software (IntelliSpace Portal, version 10.0; Philips) was used for image processing and ROI placement on the T2, T2\* maps, and DTI using the same criteria and anatomical reference images. The mean T2 and T2\* RTs, fractional anisotropy (FA), and mean diffusivity (MD) of the same muscles, cartilages, and nerves were measured at the corresponding areas.

**Statistical analysis.** Paired *t*-test was used to explore if the post-exercise values varied from the baseline imaging. Test–retest reliability between conductivities obtained from the 1st and 2nd baseline bSSFP sequences by reader I and interobserver agreement between the two readers were assessed using the intraclass correlation coefficient (ICC). An ICC of 1.0 was considered to represent perfect agreement; 0.81–0.99, almost perfect agreement; 0.61–0.80, substantial agreement; 0.41–0.60, moderate agreement; 0.21–0.40, fair agreement; and 0.20 or less, slight agreement<sup>26</sup>. All statistical analyses were performed using MedCalc version 19.0.7 (MedCalc Software Ltd). *p* values less than 0.05 were considered to indicate statistical significance.

## Results

The subjects constituted of five men and five women volunteers, ranging in age from 24 to 30 years ( $26.8 \pm 1.8$  years). The patellar and trochlear cartilages in two volunteers, were excluded on second baseline imaging due to severe artifacts. The duration of exercise ranged from 3 min 56 s to 7 min 51 s ( $6 \text{ min } 11 \text{ s} \pm 1 \text{ min } 17 \text{ s}$ ).

**Interobserver agreement and test–retest reliability.** Because there was almost perfect interobserver agreement on measurements of conductivity in muscles, cartilages, and nerves, data obtained by one of the readers were used. The result of the test–retest reliability of the baseline conductivity was almost perfect in all muscles and the tibial nerve. Cartilages tended to show lower test–retest reliability, which were regarded as substantial (Table 2).

**Baseline conductivity measurements.** The range of baseline conductivity was as follows: all muscles, 1.03–2.58 S/m; VM muscle, 1.03–1.95 S/m; SM muscle, 1.15–2.48 S/m; BF muscle, 1.45–2.58 S/m; all cartilages, 1.12–2.98 S/m; patellar cartilage, 1.11–2.80 S/m; trochlear cartilage, 1.51–2.98 S/m; tibial nerve, 1.47–3.00 S/m.

**Post-exercise changes of conductivity.** Means and standard deviations of conductivity in muscles, cartilages, and nerves during the baseline, first, and second post-exercise imaging are summarized in Table 3. Conductivity of all muscles, the BF muscle, and all cartilages on the second post-exercise imaging significantly

|                       | Test–retest reliability | Interobserver agreement |
|-----------------------|-------------------------|-------------------------|
| <b>All muscles</b>    | 0.89 (0.79–0.95)        | 0.98 (0.97–0.98)        |
| VM muscle             | 0.80 (0.41–0.95)        | 0.96 (0.93–0.98)        |
| SM muscle             | 0.96 (0.84–0.99)        | 0.97 (0.95–0.98)        |
| BF muscle             | 0.84 (0.51–0.96)        | 0.99 (0.97–0.99)        |
| <b>All cartilages</b> | 0.67 (0.28–0.87)        | 0.99 (0.98–0.99)        |
| Patellar cartilage    | 0.71 (0.09–0.94)        | 0.98 (0.97–0.99)        |
| Trochlear cartilage   | 0.64 (–0.05–0.91)       | 0.99 (0.97–0.99)        |
| <b>Tibial nerve</b>   | 0.89 (0.63–0.97)        | 0.92 (0.85–0.96)        |

**Table 2.** Test–retest reliability and interobserver agreement for conductivity measurement. Data are intraclass correlation coefficients and 95% confidence intervals in the parentheses. CI, confidence interval; VM, vastus medialis; SM, semimembranosus; BF, biceps femoris; and ICC, intraclass correlation coefficient.

|                       | Baseline    | 1st Post-exercise | 95% CI of differences* | <i>p</i> value* | 2nd Post-exercise | 95% CI of differences† | <i>p</i> value† |
|-----------------------|-------------|-------------------|------------------------|-----------------|-------------------|------------------------|-----------------|
| <b>All muscles</b>    | 1.73 ± 0.40 | 1.76 ± 0.50       | –0.05 to +0.12         | 0.428           | 1.82 ± 0.50       | +0.00 to +0.19         | 0.048           |
| VM muscle             | 1.50 ± 0.28 | 1.54 ± 0.37       | –0.08 to +0.16         | 0.482           | 1.63 ± 0.41       | –0.04 to +0.30         | 0.126           |
| SM muscle             | 1.79 ± 0.44 | 1.74 ± 0.53       | –0.23 to +0.15         | 0.626           | 1.76 ± 0.52       | –0.21 to +0.17         | 0.819           |
| BF muscle             | 1.90 ± 0.39 | 2.00 ± 0.51       | –0.06 to +0.27         | 0.191           | 2.08 ± 0.50       | +0.02 to +0.32         | 0.029           |
| <b>All cartilages</b> | 2.29 ± 0.47 | 2.18 ± 0.54       | –0.29 to +0.07         | 0.202           | 2.51 ± 0.37       | +0.07 to +0.36         | 0.006           |
| Patellar cartilage    | 2.26 ± 0.47 | 2.16 ± 0.58       | –0.38 to +0.20         | 0.483           | 2.46 ± 0.49       | –0.01 to +0.41         | 0.061           |
| Trochlear cartilage   | 2.33 ± 0.49 | 2.20 ± 0.54       | –0.41 to +0.14         | 0.299           | 2.57 ± 0.22       | –0.01 to +0.48         | 0.060           |
| <b>Tibial nerve</b>   | 2.35 ± 0.57 | 2.35 ± 0.57       | –0.20 to +0.21         | 0.953           | 2.36 ± 0.57       | –0.22 to +0.24         | 0.927           |

**Table 3.** Conductivity before and after exercise. Data are mean ± standard deviation (S/m). VM, vastus medialis; SM, semimembranosus; BF, biceps femoris; and CI, confidence interval. \*Between the baseline and 1st post-exercise MRI. †Between the baseline and 2nd post-exercise MRI.

changed by +5.41 ± 14.36% ( $p=0.048$ ), +9.05 ± 11.07% ( $p=0.029$ ), and +9.49 ± 13.69% ( $p=0.006$ ), respectively [mean ± standard deviation], with an overall increase from the baseline; conductivity of the VM muscle, patellar, and trochlear cartilages tended to increase on the second post-exercise imaging, which changed by +8.59 ± 16.12% ( $p=0.126$ ), +8.84 ± 4.13% ( $p=0.061$ ), and +10.12 ± 4.71% ( $p=0.060$ ), respectively (Figs. 2, 3, 4). All conductivities of the first post-exercise imaging and conductivity of the tibial nerve on the second post-exercise imaging were not significantly different from the baseline imaging.

**Post-exercise changes of other quantitative parameters.** After exercise, the T2 RT, T2\* RT, FA, and MD of the VM muscle changed by +17.54 ± 11.10% ( $p<0.001$ ), +19.89 ± 8.37% ( $p<0.001$ ), +5.98 ± 6.11% ( $p=0.013$ ), and +14.89 ± 4.42% ( $p<0.001$ ), respectively, with an overall increase compared to the baseline. In contrast, the BF muscle showed overall post-exercise decrease of the T2 RT, T2\* RT, and MD, which changed by –3.82 ± 4.39% ( $p=0.022$ ), –3.79 ± 4.66% ( $p=0.030$ ), and –3.59 ± 2.93% ( $p=0.004$ ) from the baseline, respectively. Regarding all muscles, overall post-exercise increase was observed in the T2\* RT and FA, which changed by +4.34 ± 11.97% ( $p=0.018$ ) and +3.52 ± 6.72% ( $p=0.012$ ) from the baseline, respectively. No other significant differences in the T2 RT, T2\* RT, FA, and MD were noted between the baseline and post-exercise imaging (Table 4).

## Discussion

This study measured *in vivo* conductivity of muscles, cartilages, and nerves around the knee joint in normal volunteers using MR-EPT and showed its feasibility. Additionally, this study revealed that post-exercise conductivity significantly changed with a tendency to increase in muscles and cartilages at 6 min after exercise cessation.

In previous animal studies, results of muscle conductivity assessment observed a large variation ranging between 0.56 and 1.05 S/m<sup>27–29</sup>, probably due to various species and study conditions. In human subjects, muscle conductivity has been reported to be 0.62 S/m<sup>30</sup> and 0.93 S/m<sup>22</sup>. In *ex vivo* studies, conductivity of cartilages and nerves were reported to be 0.51–1.14 S/m<sup>29,31</sup> and 0.39 S/m<sup>29</sup>, respectively. Though different experimental conditions make direct comparison difficult, the conductivity values of our study were higher than those of previous investigations.

Compared to the conductivity maps in previous studies on MR-EPT<sup>18,20</sup>, maps in this study were suspected to suffer from  $B_1$  inhomogeneity. The bSSFP sequence is known to have relative robustness against  $B_0$  inhomogeneity, as long as banding artifacts from signal voids are avoided, and in fact  $B_0$  inhomogeneities are too small to produce those banding artifacts in the knee images of this study; yet, conductivity reconstruction is vulnerable to  $B_1$  inhomogeneity<sup>8</sup>. Conductivity reconstruction as applied in this study is based on  $B_1$  phase only, i.e., based

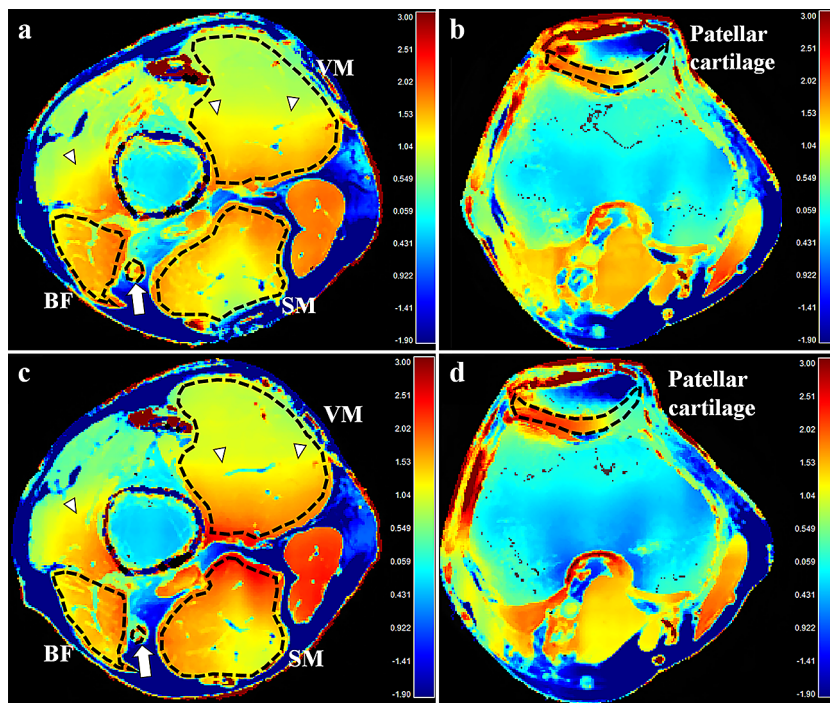


**Figure 2.** Baseline (a, b) and the post-exercise conductivity map (c, d) in a 28-year old male volunteer. Compared to the baseline, conductivity of the vastus medialis muscles and patellar cartilage increased from 1.033 to 1.188 S/m, and from 1.119 to 1.450 S/m, respectively.  $B_1$  inhomogeneity is noted across field of view, shown as demarcated areas with increased conductivity in red-colored zones (arrowheads). The unit for the scale bars is S/m. BF, biceps femoris muscle; SM, semimembranosus muscle; VM, vastus medialis muscle; arrows, tibial nerve; dotted lines, ROIs.

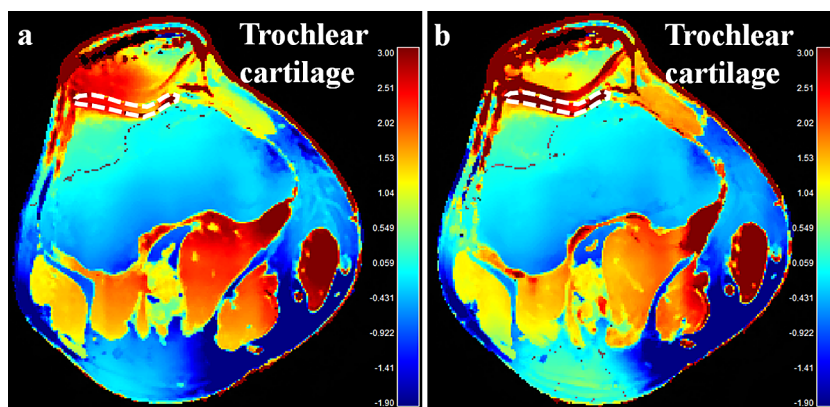


**Figure 3.** Baseline (a) and the post-exercise conductivity map (b) in a 28-year old male volunteer. Compared to the baseline, conductivity of the trochlear cartilage increased from 1.887 to 2.539 S/m. The unit for the scale bars is S/m. dotted lines, ROIs.

on the assumption of a constant  $B_1$  magnitude. It has been reported that a violation of this assumption leads to an artificial increase of reconstructed conductivity, contributing to the observed high conductivity values<sup>32</sup>. A phantom simulation as described in the Supplementary material underlines this effect, leading to roughly twice the expected conductivity as a consequence of the EPT assumptions applied. A future study shall include the additional measurement of  $B_1$  magnitude to exclude this artificial conductivity increase. Nevertheless, as  $B_1$  inhomogeneity is similar for all scans in this study, it can be expected that the observed exercise-induced increase of conductivity is not affected by this issue. Furthermore, this study adopted the so-called “transceive phase assumption”, estimating the absolute  $B_1^+$  phase  $\Phi^+$  to be half of the transceive phase  $\Phi^\pm$  as the  $B_1^+$  phase is not directly measurable by standard MR sequences<sup>15,32,33</sup>. Even though it has been widely used, violation against this assumption is thought to lower the accuracy of conductivity evaluation. Phase error has been reported to be larger

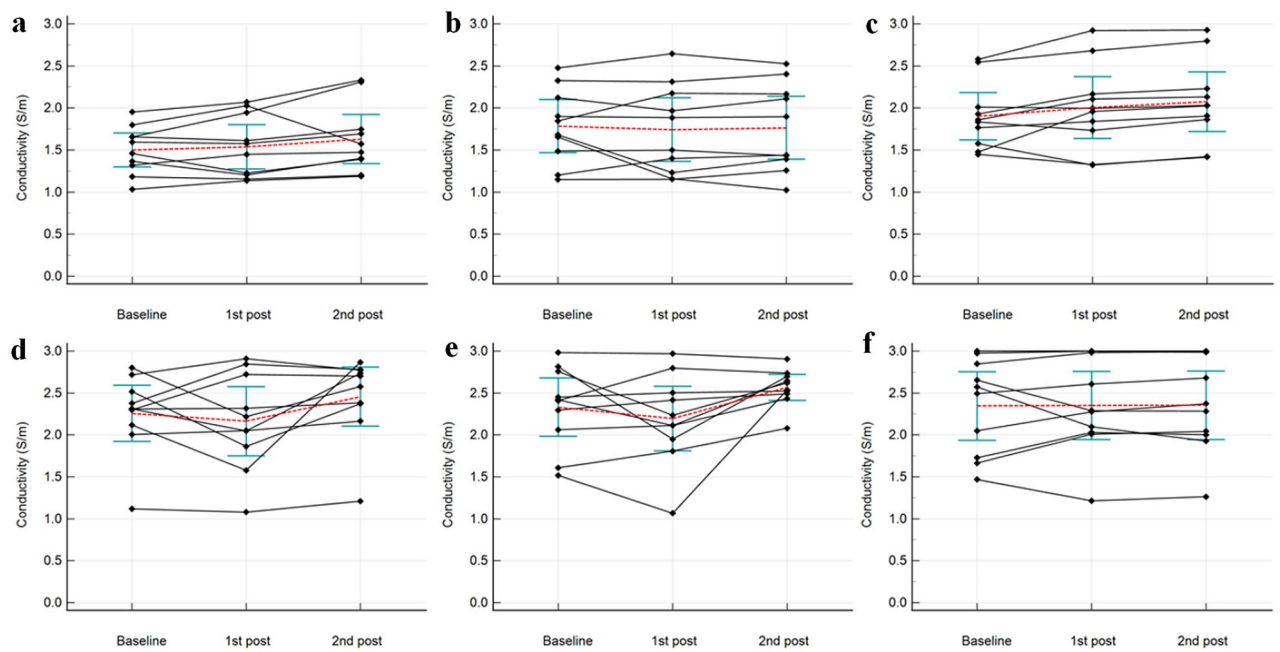


**Figure 4.** Graphs showing change of conductivity of vastus medialis muscle (a), semimembranosus muscle (b), biceps femoris muscle (c), patellar cartilage (d), trochlear cartilage (e), and tibial nerve (f) for each volunteer. The mean values are represented by red dotted lines, 95% confidence intervals of mean values by blue green bars, respectively.

at the peripheral regions indicating that the merit of this assumption deteriorates<sup>16,34</sup>. In addition, geometric asymmetry may lead to unequal contributions of the transmission and reception process in the total transeverse phase<sup>33</sup>. It can also be prone to inaccuracies when imaging subjects with asymmetrical electrical properties<sup>35</sup>. In this context, substantial phase error might have been produced in this study. As extremities are hardly scanned in the isocenter area and are inherently asymmetric with right- or left-sided predilection, this phase error could be regarded as one of the major problems to be resolved for implementing MR-EPT in musculoskeletal imaging. Given that the previous study<sup>22</sup> from which we estimated the sample size examined pelvic region, wide range of conductivity with relatively large SD in our study also might be explained by aforementioned reasons. Despite of previous study that validated MR-EPT<sup>15</sup>, our study suggests that it may be vulnerable to reconstruction error in musculoskeletal regions requiring further validation.

The post-exercise T2 and T2\* RTs, FA, and MD significantly increased in the VM muscle, which was comparable to the findings of previous studies<sup>36,37</sup>. Osmotic shift, water accumulation, increase in volume of intracellular space of perfused muscle and intracellular acidification increases T2 RT<sup>36–40</sup>, whereas blood inflow exceeding oxygen extraction fraction increases T2\* RT<sup>36,41</sup>. For DTI parameters, tightening of muscle fibers and changes in intra- and extracellular volume, pseudodiffusion due to increased blood volume are suggested to increase FA and MD, respectively<sup>40,42</sup>. In contrast, the post-exercise T2, T2\* RT, and MD of the BF muscle decreased in this study, contrary to the VM muscle. As squatting elicits greater activity of quadriceps relative to other muscles<sup>43</sup>, decreased T2, T2\* RT, and MD may imply compensatory vasoconstriction in the BF muscle.

On the other hand, conductivity tended to increase in both VM and BF muscles and cartilages on the second post-exercise MRI compared to the baseline. While conductivity is affected by both water content and tissue sodium concentration<sup>44</sup>, increased conductivity could not be explained by increased water content as T2 RT were decreased in the BF muscle and not changed in the cartilages. Thus, it could be reasonable to presume that increased conductivity may reflect increased tissue sodium concentration, which probably occurs several minutes after the exercise cessation rather than immediate post-exercise period. However, considering that the duration of exercise varied between the volunteers and that there was a difference in the pattern of change in conductivity after exercise as shown in Fig. 4, additional research is required to prove the timing of change in conductivity after exercise. In this context, exercise-induced time course changes of conductivity using a rapid sequential acquisition of MR-EPT would be another interesting topic of future investigation.

Our result showing changes of conductivity in muscle is partially comparable to those of previous studies reporting signal intensity increase of muscle after exercise using sodium MRI<sup>45,46</sup>. Whereas sodium MRI is still challenging due to limitations in hardware and software, MR-EPT is advantageous as it uses standard MR scanners. Considering usefulness of sodium MRI in evaluating early cartilage degeneration<sup>47</sup>, it could be reasonable to consider cartilage imaging as one of the promising applications of MR-EPT in the musculoskeletal regions. However, conductivity of the SM muscle did not show tendency of post-exercise increase. Although we presumed that no significant physiologic change occurred in the SM muscle after exercise considering all the other parameters were also not changed, the basis of this result remains unclear. Furthermore, the fact that the differences between baseline and post-exercise conductivity in muscles and cartilages were significant only when they were

|  | Baseline      | Post-exercise | 95% CI of difference* | p value* |
|--|---------------|---------------|-----------------------|----------|
| <b>T2 RT (ms)</b>  |               |               |                       |          |
| All muscles  | 38.39 ± 3.17  | 39.91 ± 4.29  | - 0.16 to + 3.20      | 0.074    |
| VM muscle  | 37.35 ± 1.71  | 43.90 ± 4.03  | + 3.58 to + 9.52      | < 0.001  |
| SM muscle  | 35.89 ± 1.01  | 35.50 ± 1.04  | - 1.24 to + 0.46      | 0.329    |
| BF muscle  | 41.93 ± 2.52  | 40.33 ± 1.57  | - 2.92 to - 0.28      | 0.022    |
| All cartilages   | 42.80 ± 7.71  | 42.06 ± 6.98  | - 1.81 to + 0.34      | 0.168    |
| Patellar cartilage                                       | 37.49 ± 6.04  | 37.27 ± 5.58  | - 1.17 to + 0.73      | 0.612    |
| Trochlear cartilage                                      | 48.10 ± 5.14  | 46.85 ± 4.56  | - 3.36 to + 0.86      | 0.214    |
| Tibial nerve   | 54.82 ± 5.57  | 53.93 ± 4.75  | - 2.38 to + 0.60      | 0.208    |
| <b>T2* RT (ms)</b>                                       |               |               |                       |          |
| All muscles  | 26.13 ± 1.36  | 27.61 ± 3.66  | + 0.28 to + 2.70      | 0.018    |
| VM muscle  | 26.80 ± 0.92  | 32.13 ± 2.11  | + 3.73 to + 6.93      | < 0.001  |
| SM muscle  | 25.75 ± 1.24  | 25.86 ± 1.27  | - 0.92 to + 1.14      | 0.815    |
| BF muscle  | 25.83 ± 1.67  | 24.85 ± 1.55  | - 1.84 to - 0.12      | 0.030    |
| All cartilages   | 31.56 ± 6.36  | 31.27 ± 6.15  | - 1.26 to + 0.68      | 0.538    |
| Patellar cartilage                                       | 27.05 ± 4.89  | 26.80 ± 4.82  | - 1.45 to + 0.95      | 0.648    |
| Trochlear cartilage                                      | 36.07 ± 4.03  | 35.74 ± 3.50  | - 2.12 to + 1.46      | 0.686    |
| Tibial nerve   | 25.56 ± 4.67  | 25.17 ± 5.51  | - 2.02 to + 1.24      | 0.601    |
| <b>FA</b>  |               |               |                       |          |
| All muscles  | 0.247 ± 0.035 | 0.255 ± 0.034 | + 0.002 to + 0.014    | 0.012    |
| VM muscle  | 0.234 ± 0.016 | 0.248 ± 0.017 | + 0.004 to + 0.024    | 0.013    |
| SM muscle  | 0.219 ± 0.017 | 0.227 ± 0.023 | - 0.002 to + 0.018    | 0.104    |
| BF muscle  | 0.287 ± 0.021 | 0.289 ± 0.027 | - 0.012 to + 0.016    | 0.751    |
| All cartilages   | 0.134 ± 0.042 | 0.124 ± 0.030 | - 0.028 to + 0.009    | 0.298    |
| Patellar cartilage                                       | 0.129 ± 0.038 | 0.113 ± 0.017 | - 0.039 to + 0.007    | 0.149    |
| Trochlear cartilage                                      | 0.138 ± 0.047 | 0.135 ± 0.036 | - 0.037 to + 0.031    | 0.844    |
| Tibial nerve   | 0.539 ± 0.011 | 0.552 ± 0.048 | - 0.054 to + 0.080    | 0.672    |
| <b>MD (<math>\times 10^{-3}</math> mm<sup>2</sup>/s)</b> |               |               |                       |          |
| All muscles  | 1.57 ± 0.08   | 1.59 ± 0.26   | - 0.06 to + 0.11      | 0.570    |
| VM muscle  | 1.63 ± 0.06   | 1.87 ± 0.05   | + 0.19 to + 0.29      | < 0.001  |
| SM muscle  | 1.52 ± 0.06   | 1.41 ± 0.27   | - 0.33 to + 0.10      | 0.269    |
| BF muscle  | 1.56 ± 0.10   | 1.51 ± 0.08   | - 0.09 to - 0.02      | 0.004    |
| All cartilages   | 1.68 ± 0.14   | 1.66 ± 0.23   | - 0.15 to + 0.09      | 0.645    |
| Patellar cartilage                                       | 1.69 ± 0.14   | 1.62 ± 0.30   | - 0.30 to + 0.16      | 0.530    |
| Trochlear cartilage                                      | 1.68 ± 0.14   | 1.70 ± 0.12   | - 0.10 to + 0.13      | 0.792    |
| Tibial nerve   | 1.15 ± 0.16   | 1.08 ± 0.16   | - 0.19 to + 0.05      | 0.246    |

**Table 4.** Quantitative measurements before and after exercise. Data are mean ± standard deviation. VM, vastus medialis; SM, semimembranosus; BF, biceps femoris; RT, relaxation time; FA, fractional anisotropy; MD, mean diffusivity; and CI, confidence interval. \*Between the baseline and post-exercise MRI.

grouped except for the BF muscle requires future investigation to elucidate its true significance. In addition to the technical issues regarding  $B_1$  inhomogeneity, relatively low test–retest reliability in the cartilage possibly due to their small size and curved shape is another hurdle that should be overcome.

This study had several limitations. First, the MR-EPT technique was not validated in the musculoskeletal regions. Validation using a knee-sized phantom and conductivity probe could help proving its reliability in musculoskeletal imaging. Second, substantial inhomogeneity was noted in the conductivity maps with regions of increased conductivity, as described above. Further optimization would be mandatory, which may provide conductivity values closer to the values reported in previous investigations. Third, the time intervals between exercise cessation and acquisition of each sequence for quantitative measurements were variable. The duration of exercise was also variable among the volunteers, which also may have influenced the study results particularly in post-exercise changes of conductivity. Fourth, misalignment of knee joints between the baseline and post-exercise scans could have been possible. Intelligent software which automatically plans the scanning geometries would be helpful, in addition to our effort using skin marking and integrated laser. Finally, temperature measurements of target tissues were not performed, assuming them to be 37 °C for both baseline and post-exercise MRI. As temperature coefficient of conductivity variation is about 2%/°C<sup>48</sup>, change of temperature after exercise may have affected our study results.



In conclusion, in vivo conductivity measurement was feasible in musculoskeletal tissues using MR-EPT around the knee joint. Although technological hurdles should be overcome that might result in artificial increase of conductivity values and relatively poor reproducibility of cartilage conductivity, significant post-exercise change in conductivity may suggest its potential as a biomarker to reflect physiologic status of musculoskeletal tissues. Further clinical studies with validation based on this initial experience of MR-EPT would be mandatory to elucidate true significance of conductivity in musculoskeletal imaging and to expand its applications particularly to indirect assessment of tissue sodium concentration.

Received: 4 February 2021; Accepted: 10 December 2021

Published online: 07 January 2022

## References

- Kandadai, M. A., Raymond, J. L. & Shaw, G. J. Comparison of electrical conductivities of various brain phantom gels: Developing a 'brain gel model'. *Mater. Sci. Eng. C-Mater.* **32**, 2664–2667. <https://doi.org/10.1016/j.msec.2012.07.024> (2012).
- Gabriel, S., Lau, R. W. & Gabriel, C. The dielectric properties of biological tissues: II. Measurements in the frequency range 10 Hz to 20 GHz. *Phys. Med. Biol.* **41**, 2251–2269. <https://doi.org/10.1088/0031-9155/41/11/002> (1996).
- Hurt, W. D. Multiterm Debye dispersion relations for permittivity of muscle. *IEEE Trans. Biomed. Eng.* **32**, 60–64. <https://doi.org/10.1109/TBME.1985.325629> (1985).
- Surowiec, A. J., Stuchly, S. S., Barr, J. B. & Swarup, A. Dielectric properties of breast carcinoma and the surrounding tissues. *IEEE Trans. Biomed. Eng.* **35**, 257–263. <https://doi.org/10.1109/10.1374> (1988).
- Jossinet, J. The impedivity of freshly excised human breast tissue. *Physiol. Meas.* **19**, 61–75. <https://doi.org/10.1088/0967-3334/19/1/006> (1998).
- Fallert, M. A. *et al.* Myocardial electrical impedance mapping of ischemic sheep hearts and healing aneurysms. *Circulation* **87**, 199–207. <https://doi.org/10.1161/01.cir.87.1.199> (1993).
- Haemmerich, D. *et al.* In vivo electrical conductivity of hepatic tumours. *Physiol. Meas.* **24**, 251–260. <https://doi.org/10.1088/0967-3334/24/2/302> (2003).
- Katscher, U., Kim, D. H. & Seo, J. K. Recent progress and future challenges in MR electric properties tomography. *Comput. Math. Methods Med.* **2013**, 546562. <https://doi.org/10.1155/2013/546562> (2013).
- Zhang, X., Liu, J. & He, B. Magnetic-resonance-based electrical properties tomography: a review. *IEEE Rev. Biomed. Eng.* **7**, 87–96. <https://doi.org/10.1109/RBME.2013.2297206> (2014).
- Holder, D. S. *Electrical Impedance Tomography: Methods, History and Applications* (Institute of Physics Publishing, 2005).
- Seo, J. K., Yoon, J. R., Woo, E. J. & Kwon, O. Reconstruction of conductivity and current density images using only one component of magnetic field measurements. *IEEE Trans. Biomed. Eng.* **50**, 1121–1124. <https://doi.org/10.1109/Tbme.2003.816080> (2003).
- Korzhenevskii, A. V. & Cherepenin, V. A. Magnetic induction tomography. *Radiotekh. Elektron. (Moscow)* **42**, 506–512 (1997).
- Haacke, E., Petropoulos, L., Nilges, E. & Wu, D. Extraction of conductivity and permittivity using magnetic resonance imaging. *Phys. Med. Biol.* **36**, 723 (1991).
- Katscher, U., Hanft, M., Vernickel, P. & Findekle, C. Electric properties tomography (EPT) via MRI. *Proc. Intl. Soc. Mag. Reson. Med.* **14** (2006).
- Katscher, U. *et al.* Determination of electric conductivity and local SAR via B1 mapping. *IEEE Trans. Med. Imaging* **28**, 1365–1374. <https://doi.org/10.1109/TMI.2009.2015757> (2009).
- Balidemaj, E. *et al.* Feasibility of electric property tomography of pelvic tumors at 3T. *Magn. Reson. Med.* **73**, 1505–1513. <https://doi.org/10.1002/mrm.25276> (2015).
- Voigt, T., Homann, H., Katscher, U. & Doessel, O. Patient-individual local SAR determination: In vivo measurements and numerical validation. *Magn. Reson. Med.* **68**, 1117–1126. <https://doi.org/10.1002/mrm.23322> (2012).
- Mori, N. *et al.* Diagnostic value of electric properties tomography (EPT) for differentiating benign from malignant breast lesions: Comparison with standard dynamic contrast-enhanced MRI. *Eur. Radiol.* **29**, 1778–1786. <https://doi.org/10.1007/s00330-018-5708-4> (2019).
- Kim, S. Y. *et al.* Correlation between conductivity and prognostic factors in invasive breast cancer using magnetic resonance electric properties tomography (MREPT). *Eur. Radiol.* **26**, 2317–2326. <https://doi.org/10.1007/s00330-015-4067-7> (2016).
- Tha, K. K. *et al.* Noninvasive electrical conductivity measurement by MRI: A test of its validity and the electrical conductivity characteristics of glioma. *Eur. Radiol.* **28**, 348–355. <https://doi.org/10.1007/s00330-017-4942-5> (2018).
- Stehning, C., Voigt, T., Karkowski, P. & Katscher, U. Electric properties tomography (EPT) of the liver in a single breathhold using SSFP. *Proc. Intl. Soc. Mag. Reson. Med.* **20**, abstract 386 (2012).
- Balidemaj, E. *et al.* In vivo electric conductivity of cervical cancer patients based on B(1)(+) maps at 3T MRI. *Phys. Med. Biol.* **61**, 1596–1607. <https://doi.org/10.1088/0031-9155/61/4/1596> (2016).
- Liess, C., Lusse, S., Karger, N., Heller, M. & Gluer, C. C. Detection of changes in cartilage water content using MRI T2-mapping in vivo. *Osteoarthr. Cartil.* **10**, 907–913. <https://doi.org/10.1053/joca.2002.0847> (2002).
- Park, J. E. *et al.* Low conductivity on electrical properties tomography demonstrates unique tumor habitats indicating progression in glioblastoma. *Eur. Radiol.* **31**, 6655–6665. <https://doi.org/10.1007/s00330-021-07976-w> (2021).
- Suh, J. *et al.* Noncontrast-enhanced MR-based conductivity imaging for breast cancer detection and lesion differentiation. *J. Magn. Reson. Imaging* **54**, 631–645. <https://doi.org/10.1002/jmri.27655> (2021).
- Landis, J. R. & Koch, G. G. The measurement of observer agreement for categorical data. *Biometrics* **33**, 159–174 (1977).
- Oswald, K. Messung der leitfähigkeit und Dielektrizitätskonstante biologischer Gewebe und Flüssigkeiten bei kurzen Wellen. *Hochfreq. Tech. Elektroakust.* **49**, 40–49 (1937).
- Stoy, R. D., Foster, K. R. & Schwan, H. P. Dielectric properties of mammalian tissues from 0.1 to 100 MHz: A summary of recent data. *Phys. Med. Biol.* **27**, 501–513. <https://doi.org/10.1088/0031-9155/27/4/002> (1982).
- Gabriel, C. & Gabriel, S. *Compilation of the Dielectric Properties of Body Tissues at RF and Microwave Frequencies* (Dept of Physics, King's Coll, 1996).
- Joines, W. T., Zhang, Y., Li, C. & Jirtle, R. L. The measured electrical properties of normal and malignant human tissues from 50 to 900 MHz. *Med. Phys.* **21**, 547–550. <https://doi.org/10.1118/1.597312> (1994).
- Binette, J. S., Garon, M., Savard, P., McKee, M. D. & Buschmann, M. D. Tetrapolar measurement of electrical conductivity and thickness of articular cartilage. *J. Biomech. Eng.* **126**, 475–484. <https://doi.org/10.1115/1.1785805> (2004).
- Voigt, T., Katscher, U. & Doessel, O. Quantitative conductivity and permittivity imaging of the human brain using electric properties tomography. *Magn. Reson. Med.* **66**, 456–466. <https://doi.org/10.1002/mrm.22832> (2011).
- van Lier, A. L. *et al.* B1(+) phase mapping at 7 T and its application for in vivo electrical conductivity mapping. *Magn. Reson. Med.* **67**, 552–561. <https://doi.org/10.1002/mrm.22995> (2012).

34. van Lier, A. L. *et al.* Electrical properties tomography in the human brain at 1.5, 3, and 7T: A comparison study. *Magn. Reson. Med.* **71**, 354–363. <https://doi.org/10.1002/mrm.24637> (2014).
35. Liu, J., Zhang, X., Schmitter, S., Van de Moortele, P. F. & He, B. Gradient-based electrical properties tomography (gEPT): A robust method for mapping electrical properties of biological tissues in vivo using magnetic resonance imaging. *Magn. Reson. Med.* **74**, 634–646. <https://doi.org/10.1002/mrm.25434> (2015).
36. Varghese, J. *et al.* Rapid assessment of quantitative T1, T2 and T2\* in lower extremity muscles in response to maximal treadmill exercise. *NMR Biomed.* **28**, 998–1008. <https://doi.org/10.1002/nbm.3332> (2015).
37. Patten, C., Meyer, R. A. & Fleckenstein, J. L. T2 mapping of muscle. *Semin. Musculoskelet. Radiol.* **7**, 297–305. <https://doi.org/10.1055/s-2004-815677> (2003).
38. Damon, B. M. *et al.* Intracellular acidification and volume increases explain R2 decreases in exercising muscle. *Magn. Reson. Med.* **47**, 14–23. <https://doi.org/10.1002/mrm.10043> (2002).
39. Louie, E. A., Gochberg, D. F., Does, M. D. & Damon, B. M. Transverse relaxation and magnetization transfer in skeletal muscle: effect of pH. *Magn. Reson. Med.* **61**, 560–569. <https://doi.org/10.1002/mrm.21847> (2009).
40. Nakai, R. *et al.* MRI analysis of structural changes in skeletal muscles and surrounding tissues following long-term walking exercise with training equipment. *J. Appl. Physiol.* **105**, 958–963. <https://doi.org/10.1152/jappphysiol.01204.2007> (2008).
41. Andreisek, G. *et al.* T2\*-weighted and arterial spin labeling MRI of calf muscles in healthy volunteers and patients with chronic exertional compartment syndrome: Preliminary experience. *AJR Am. J. Roentgenol.* **193**, W327–333. <https://doi.org/10.2214/AJR.08.1579> (2009).
42. Oudeman, J. *et al.* Techniques and applications of skeletal muscle diffusion tensor imaging: A review. *J. Magn. Reson. Imaging* **43**, 773–788. <https://doi.org/10.1002/jmri.25016> (2016).
43. Escamilla, R. F. *et al.* Biomechanics of the knee during closed kinetic chain and open kinetic chain exercises. *Med. Sci. Sports Exerc.* **30**, 556–569. <https://doi.org/10.1097/00005768-199804000-00014> (1998).
44. van Lier, A. L. H. M. W. *et al.* 23Na-MRI and EPT: Are sodium concentration and electrical conductivity at 298 MHz (7T) related? *Proc. Intl. Soc. Mag. Reson. Med.* **21**, abstract 0115 (2013).
45. Hammon, M. *et al.* 3 Tesla (23)Na magnetic resonance imaging during aerobic and anaerobic exercise. *Acad. Radiol.* **22**, 1181–1190. <https://doi.org/10.1016/j.acra.2015.06.005> (2015).
46. Chang, G., Wang, L., Schweitzer, M. E. & Regatte, R. R. 3D 23Na MRI of human skeletal muscle at 7 Tesla: Initial experience. *Eur. Radiol.* **20**, 2039–2046. <https://doi.org/10.1007/s00330-010-1761-3> (2010).
47. Zbyn, S. *et al.* Assessment of low-grade focal cartilage lesions in the knee with sodium MRI at 7 T: Reproducibility and short-term, 6-month follow-up data. *Invest. Radiol.* **55**, 430–437. <https://doi.org/10.1097/RLI.0000000000000652> (2020).
48. Leussler, C., Karkowski, P. & Katscher, U. Temperature dependant conductivity change using MR based electric properties tomography. *Proc. Intl. Soc. Mag. Reson. Med.* **20**, 3451 (2012).

## Acknowledgements

The authors thank Lukas Hildebrand for providing simulation data used in the Supplementary material.

## Author contributions

J.H.L. collected data, conducted all statistical analyses and wrote the manuscript. Y.C.Y. conceived, designed, and supervised the study. H.S.K. substantially revised the manuscript. J.L. analyzed data. E.K. developed the study design and helped with the technical implementation of the sequences. C.F. conducted the simulation test. U.K. processed the data and wrote the manuscript. All authors reviewed and approved the manuscript.

## Funding

Samsung Medical Center (Grant No. SMO1200281).

## Competing interests

This work was supported by research funding of Samsung Medical Center (No. SMO1200281). Three authors of this manuscript (E.K., C.F., and U.K.) are employees of Philips. All the other authors (J.H.L., Y.C.Y., H.S.K., J.L.) declare no competing interests.

## Additional information

**Supplementary Information** The online version contains supplementary material available at <https://doi.org/10.1038/s41598-021-03928-y>.

**Correspondence** and requests for materials should be addressed to Y.C.Y.

**Reprints and permissions information** is available at [www.nature.com/reprints](http://www.nature.com/reprints).

**Publisher's note** Springer Nature remains neutral with regard to jurisdictional claims in published maps and institutional affiliations.



**Open Access** This article is licensed under a Creative Commons Attribution 4.0 International License, which permits use, sharing, adaptation, distribution and reproduction in any medium or format, as long as you give appropriate credit to the original author(s) and the source, provide a link to the Creative Commons licence, and indicate if changes were made. The images or other third party material in this article are included in the article's Creative Commons licence, unless indicated otherwise in a credit line to the material. If material is not included in the article's Creative Commons licence and your intended use is not permitted by statutory regulation or exceeds the permitted use, you will need to obtain permission directly from the copyright holder. To view a copy of this licence, visit <http://creativecommons.org/licenses/by/4.0/>.

© The Author(s) 2022, corrected publication 2022